Comparisons of finite element and Rayleigh methods for the study of conical Bloch waves in arrays of metallic cylinders

S. Guenneau
Blackett Laboratory, Imperial College London, London, UK
A. Nicolet
Institut Fresnel, Université Aix-Marseille III, Marseille, France
C. Geuzaine
California Institute of Technology, Applied and Computational Mathematics, Pasadena, California, USA
F. Zolla
Institut Fresnel, Université Aix-Marseille I, Marseille, France
A.B. Movchan
Department of Mathematical Sciences, Liverpool, UK

Keywords *Communication technologies, Finite element analysis, Numerical analysis*

Abstract *This paper investigates new technological devices to be utilised in future optical communications, by means of variational method (FEM) and multipole scattering approach (Rayleigh method). This last one provides interesting asymptotic results in the long-wavelength limit. The so-called photonic crystal fibres (PCF) possess radically different guiding properties due to photonic band gap guidance: removing a hole within a macro-cell leads to a defect state within the gap. In the case of multi-core PCF, the localised modes start talking to each other which possibly leads to a new generation of multiplexer/demultiplexers.*

1. Introduction

Nanostructured materials containing ordered arrays of cylindrical holes pave the way of an optoelectronics revolution, doing for light what silicon did for electrons. The microelectronics revolution was based on the elaborate control of electric currents achieved with semiconductors as silicon. That control depends on a phenomenon called the band gap, i.e. a range of energies in which electrons are blocked from travelling through the semiconductor. By analogy with semiconductors, physicist have produced materials with a photonic band gap – a range of wavelengths of light that is blocked by the material – by structuring the material in carefully designed patterns at the nanoscopic-size scale. These so-called photonic crystals (PC) act as semiconductors for light and promise innumerable technological applications. Such structures can be stretched along the third dimension, forming a new kind of optical fibres, christened "photonic crystal fibres" (PCF). Conventional optical fibres have a high refractive index

COMPEL: The International Journal for Computation and Mathematics in Electrical and Electronic Engineering
Vol. 23 No. 4, 2004
pp. 932-949

0332-1649
DOI 10.1108/03321640410553364

S. Guenneau acknowledges support from DoD/ONR MURI grant N00014-01-1-0803. C. Geuzaine is a Postdoctoral Researcher with the Belgian National Fund for Scientific Research.

at their core, which confines light by total internal reflection. Philip St J. Russell of the University of Bath in England demonstrated in 1999 how to make photonic band-gap fibres (Knight *et al.*, 1999). In one version, light travels along a central hole in the fibre, confined there by the two-dimensional band gap of a surrounding periodic cladding. More optical power can be sent through such a central void than through glass, enabling greater information-carrying capacity, perhaps 100 times that of conventional telecommunications fibres. Specialty fibres have advanced the most as commercial photonic band-gap products. Two companies, one of them being based in UK ("www.blazephotonics.com") and led by Philip St J. Russell, have already distributed sample quantities and will soon begin volume production of PCF. We present analysis of electromagnetic waves propagating through such doubly periodic array of cylindrical channels in oblique incidence. We use Floquet-Bloch quasi-periodicity conditions to take into account the periodicity of the problem (Nicolet *et al.*, 2004). Although one may argue that the PCF reportedly have a finite size in real world (Knight *et al.*, 1999), this model enables us to construct dispersion curves for the corresponding periodic structure. We exhibit band gaps in conical incidence and study localised modes associated with a defect in a macrocell.

2. Rayleigh method

2.1 Set up of the spectral problem

2.1.1 Maxwell's equations at work. We consider a periodic heterogeneous lossless medium. This micro-structure is characterised by its permittivity $\varepsilon = \varepsilon_r \varepsilon_0$ (ε_0 is the permittivity of vacuum) and its permeability $\mu = \mu_r \mu_0$ (μ_0 is the permeability of vacuum). We assume an implicit time dependence $\exp(-i\omega t)$ of the electric field $\underline{\mathbf{E}}(x, y, z)$ and the magnetic field $\underline{\mathbf{H}}(x, y, z)$, which are therefore solutions of the time harmonic Maxwell's equations (in the sense of distributions in $\mathbb{R}^3$):

$$\begin{cases} \operatorname{curl} \underline{\mathbf{E}} = i\omega\mu_0\mu_r \underline{\mathbf{H}}, & \operatorname{div}(\varepsilon_r \underline{\mathbf{E}}) = 0 \\ \operatorname{curl} \underline{\mathbf{H}} = -i\omega\varepsilon_0\varepsilon_r \underline{\mathbf{E}}, & \operatorname{div}(\mu_r \underline{\mathbf{H}}) = 0 \end{cases} \tag{1}$$

Since we are studying propagation of modes in a periodic medium, the well posedness of this spectral problem is ensured by the Floquet-Bloch quasi-periodicity conditions which hold on the boundary of a basic cell (provided that ε_r and μ_r are real functions with strictly positive lower and upper bounds).

In the case of propagating waves in conical incidence in a medium invariant along the z-axis, $\underline{\mathbf{V}}$ ($\underline{\mathbf{V}}$ denoting either $\underline{\mathbf{E}}$ or $\underline{\mathbf{H}}$) is sought in the form:

$$\underline{\mathbf{V}} = \mathbf{V}(r, \Phi)\, e^{i\gamma z}, \tag{2}$$

where γ is the (strictly positive) propagation constant and r and Φ denote the radial and angular variables of $\mathbf{V}$ which is associated with one of the basic cells (Figure 1), which we denote as $Y = [0; d] \times [0; d]$ (d is the pitch of the square array).

From now on, we will study piecewise-constant permittivity and permeability: we restrict our analysis to the important case of a periodic assembly of infinite conducting cylindrical inclusions of circular cross-section C (Knight *et al.*, 1999). Using the vector Helmholtz decomposition

$$\operatorname{curl}(\operatorname{curl} \underline{\mathbf{V}}) = -\Delta \underline{\mathbf{V}} + \operatorname{grad}(\operatorname{div} \underline{\mathbf{V}}), \tag{3}$$

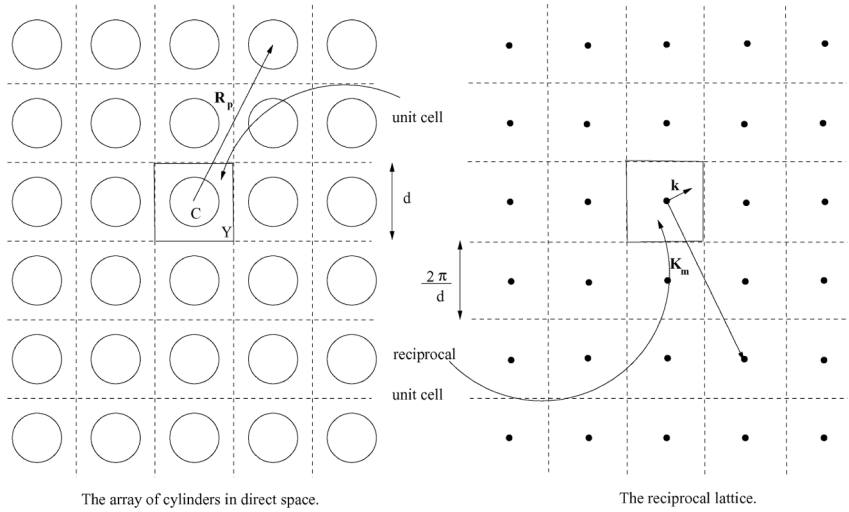

Figure 1.
Physical space and reciprocal space

we find that in the medium between the metallic inclusions, the electric and magnetic field satisfies the vector Helmholtz equation

$$(\Delta + k^2)\underline{\mathbf{V}} = 0, \tag{4}$$

where the spectral parameter k denotes $\sqrt{\omega^2 \varepsilon_0 \varepsilon_r \mu_0 \mu_r}$, ε_r and μ_r being, respectively, the relative permittivity and permeability in the matrix.

Because the rods are infinitely extended in the z-direction, the x and y components of the $\mathbf{E}$ and $\mathbf{H}$ fields can be reconstructed from their z-components, via the equations

$$\underline{\mathbf{E}}_t = \frac{1}{\varepsilon_0 \varepsilon_r \mu_0 \mu_r \omega^2 - \gamma^2}(\mathrm{i}\gamma \mathrm{grad}_t \underline{E}_z - \mathrm{i}\omega\mu_r \mathbf{e}_z \times \mathrm{grad}_t \underline{H}_z), \tag{5}$$

$$\underline{\mathbf{H}}_t = \frac{1}{\varepsilon_0 \varepsilon_r \mu_0 \mu_r \omega^2 - \gamma^2}(\mathrm{i}\gamma \mathrm{grad}_t \underline{H}_z + \mathrm{i}\omega\varepsilon_r \mathbf{e}_z \times \mathrm{grad}_t \underline{E}_z). \tag{6}$$

It should be noted that in the subsequent analysis we retain the z-dependence of the fields.

The mathematical model of infinite conducting inclusions amounts to assuming that the tangential part of the electric field $\mathbf{n} \times \mathbf{E}$ be vanishing on their boundary, unlike the tangential part of the magnetic field $\mathbf{n} \times \mathbf{H}$ which involves the (unknown) current. If we write the tangent vector at any given point on the inclusion surface ∂C as $\mathbf{e}_\tau$ and the normal vector as $\mathbf{n}$ then

$$\mathbf{n} \times \underline{\mathbf{E}}|_{\partial C} = \left\{ \underline{E}_z \mathbf{e}_\tau + \mathbf{e}_z \times \left(\frac{\mathrm{i}\gamma}{\varepsilon_r \mu_r \omega^2 - \gamma^2} \frac{\partial \underline{E}_z}{\partial \tau} - \frac{\mathrm{i}\omega\mu_r}{\varepsilon_r \mu_r \omega^2 - \gamma^2} \frac{\partial \underline{H}_z}{\partial n} \right) \right\} \Bigg|_{\partial C} = 0. \tag{7}$$

2.1.2 Conical mounting for metallic cylinders: miracle making. Noting that $\mathbf{e}_\tau$ and $\mathbf{e}_z$ are perpendicular, we can express the boundary conditions as a set of restrictions on the z-components of the fields. These are

$$\underline{E}_z|_{\partial C} = 0, \tag{8}$$

$$\left(\frac{\mathrm{i}\gamma}{\varepsilon_r\mu_r\omega^2 - \gamma^2}\frac{\partial \underline{E}_z}{\partial \tau} - \frac{\mathrm{i}\omega\mu_r}{\varepsilon_r\mu_r\omega^2 - \gamma^2}\frac{\partial \underline{H}_z}{\partial n}\right)\Bigg|_{\partial C} = 0. \tag{9}$$

When $\gamma = 0$, it follows straightforwardly from (9) that

$$\left.\frac{\partial \underline{H}_z}{\partial n}\right|_{\partial C} = 0. \tag{10}$$

So that we can split the problem into two fundamental polarisations in the sense that every field can be expressed as two decoupled fields, namely a T.E. field for which H_z is the solution of

$$(\Delta + k^2)H_z = 0, \quad \text{outside the metal,} \tag{11}$$

$$\left.\frac{\partial H_z}{\partial n}\right|_{\partial C} = 0, \quad \text{on the boundary of each cylinder,} \tag{12}$$

and a T.M. field for which E_z is the solution of

$$(\Delta + k^2)E_z = 0, \quad \text{outside the metal,} \tag{13}$$

$$E_z|_{\partial C} = 0, \quad \text{on the boundary of each cylinder.} \tag{14}$$

When $\gamma > 0$, the boundary conditions in equations (8) and (10) still hold, which is one of the peculiarities shared by the model of infinitely conducting metallic cylinders. The fact that the conical mounting does not mix the polarisations is certainly not trivial (and actually not true for dielectric cylinders). Hence, we thought that this remarkable fact deserves a little digression from the main stream of the paper.

If $0 < \gamma \ll 1$, we can assume that $\underline{E}_z$ and $\underline{H}_z$ are represented in the form

$$\underline{E}_z(\omega, \gamma) = \underline{E}_z^0(\omega) + \gamma\underline{E}_z^1(\omega) + \mathcal{O}(\gamma^2), \tag{15}$$

$$\underline{H}_z(\omega, \gamma) = \underline{H}_z^0(\omega) + \gamma\underline{H}_z^1(\omega) + \mathcal{O}(\gamma^2). \tag{16}$$

If we neglect all terms of order $\mathcal{O}(\gamma^2)$, the boundary condition in equation (9) implies that equation (10) is first order in γ.

Now, if $\gamma \gg 1$, $\underline{E}_z$ and $\underline{H}_z$ are represented in the form

$$\underline{E}_z(\omega, \gamma) = \gamma^{-1}\underline{E}_z^1(\omega) + \gamma^{-2}\underline{E}_z^2(\omega) + \mathcal{O}(\gamma^{-3}), \tag{17}$$

$$\underline{H}_z(\omega, \gamma) = \gamma^{-1}\underline{H}_z^1(\omega) + \gamma^{-2}\underline{H}_z^2(\omega) + \mathcal{O}(\gamma^{-3}). \tag{18}$$

If we neglect all terms of order $\mathcal{O}(\gamma^{-3})$, the boundary condition in equation (9) implies

$$\left.\frac{\partial \underline{E}_z}{\partial \tau}\right|_{\partial C} = 0$$

to order γ^{-2} which brings a trivial result. What saves us is the boundary condition in equation (8) which in any case (for every $\gamma > 0$) ensures us that equation (9) leads to equation (10)!

But that is not all, we should also note that equations (8) and (10) hold both for ($\underline{E}_z$, $\underline{H}_z$) and (E_z,H_z) due to the definition (2) and the fact that $\mathbf{n}$ is perpendicular to the z-axis.

2.1.2 Recast of the problem into longitudinal components. Finally, the boundary value problem splits in two fundamental polarisations, namely T.E. polarisation

$$(\Delta + k_\perp^2)H_z = 0, \quad \text{outside the metal,} \tag{19}$$

$$\left.\frac{\partial H_z}{\partial n}\right|_{\partial C} = 0, \quad \text{on the boundary of each cylinder} \tag{20}$$

and T.M. polarisation

$$(\Delta + k_\perp^2)E_z = 0, \quad \text{outside the metal,} \tag{21}$$

$$E_z|_{\partial C} = 0, \quad \text{on the boundary of each cylinder} \tag{22}$$

with $k_\perp = \sqrt{\omega^2 \varepsilon_0 \varepsilon_r \mu_0 \mu_r - \gamma^2}$. It should be noted that ω should be greater than the so-called cut-off frequency $\omega_c = \gamma/\sqrt{\varepsilon_0 \varepsilon_r \mu_0 \mu_r}$ to ensure a real (positive) transverse wave-number $k_\perp$.

2.1.3 The Bloch conditions: from boundary value to spectral problems. For the spectral problem to be completely specified, we further assume that the longitudinal part V_z of the vector field $\mathbf{V}$ satisfies an appropriate quasi-periodicity condition known as the Floquet-Bloch condition

$$\mathbf{V}(\mathbf{r} + \mathbf{R_p}) = \mathbf{V}(\mathbf{r})e^{i\mathbf{k}\cdot\mathbf{R_p}}, \tag{23}$$

where $\mathbf{k}$ is known as the Bloch wave-vector and $\mathbf{R_p} = p_1\mathbf{a}^1 + p_2\mathbf{a}^2$ is the vector attached to the nodes $\mathbf{p} = (p_1, p_2) \in \mathbf{Z}^2$ of the lattice of translations vectors $\mathbf{a}^1$ and $\mathbf{a}^2$, which form the basis for the lattice as a whole (Figure 1).

2.1.4 An orphan: the TEM case. Most of the studies dealing with the infinite array of metallic cylinders light-heartedly skip the important issue of the most peculiar class of so-called transverse electric-magnetic waves, except in the noticeable work of McPhedran *et al.* (1997). These modes are of the form (2) but otherwise they should also fullfil the restrictive condition

$$E_z = 0, \quad H_z = 0, \tag{24}$$

within the PCF. Let us check whether or not such a constraint is achievable.

Firstly, it follows from either equation (5) or (6) together with equation (24) that the propagation constant γ has to be equal to the wavenumber $k = \omega\sqrt{\varepsilon_0 \varepsilon_r \mu_0 \mu_r}$ if we want non zero $\mathbf{E}_t$ or $\mathbf{H}_t$. Hence, in the transverse case ($\gamma = 0$) TEM modes would only stand a chance to exist in the static limit.

Secondly, plugging $\underline{\mathbf{E}} = \mathbf{E}_t\, e^{i\gamma z}$ and $\underline{\mathbf{H}} = \mathbf{H}_t e^{i\gamma z}$ in equation (1), we find

$$\mathrm{curl}\,\underline{\mathbf{E}} = (\mathrm{curl}\,\mathbf{E}_t + i\gamma \mathbf{e}_z \times \mathbf{E}_t)e^{i\gamma z} = i\omega\mu_0\mu_r \underline{\mathbf{H}}_t \tag{25}$$

The second equality in equation (25) holds true if and only if $\mathrm{curl}\,\mathbf{E}_t = 0$ in the sense of distributions, since both $\mathbf{H}_t$ and $\mathbf{e}_z \times \mathbf{E}_t$ are orthogonal to $\mathbf{e}_z$ unlike $\mathrm{curl}\,\mathbf{E}_t$ which is

colinear to $\mathbf{e}_z$. Owing to equation (20), (22) and (24) $\mathbf{E}_t|_{\partial C}$ is also null. Hence, $\mathbf{E}_t$ is irrotational in classical sense and it therefore derives from a potential W_{TE}:

$$\mathbf{E}_t = -\mathrm{grad}\, W_{\mathrm{TE}}, \quad \text{in } Y\backslash\bar{C} \tag{26}$$

A similar reasoning can be led for $\mathbf{H}_t$ but we notice that only its normal derivative will vanish of the boundary C and therefore it is only irrotational in distributional sense (due to the existence of a current $\mathbf{n}\times\mathbf{H}_t$ on ∂C). Now, from equations (1) and (26), we have

$$\Delta W_{\mathrm{TE}} = \mathrm{div}(\mathrm{grad}\, W_{\mathrm{TE}}) = -\mathrm{div}\,\mathbf{E}_t = 0, \quad \text{in } Y\backslash\bar{C}, \tag{27}$$

both in distributional and classical sense (due to Dirichlet boundary conditions on ∂C).

At this stage, we remark that $Y\backslash\bar{C}$ is a not simply connected set (it would be simply connected if we would consider an array of dielectric cylinders). Therefore, equation (27) does not imply that the (quasi-periodic) potential W_{TE} be constant over the basic cell (which would lead to $\mathbf{E}_t = 0$). It is important to note also that the potential W_{TE} is bound to take a value W^i_{TE} on the boundary ∂C in the ith basic cell within the array which is distinct from its value W^j_{TE} on the boundary ∂C in the jth basic cell if $i \neq j$. We are therefore in presence of a quasi-periodic potential solution of a problem of electrostatic type. The analysis of the quasi-static limit led by Poulton *et al.* (2001) reveals the following relationships between on the one hand, the dynamic field quantities H_z and our electrostatic potential W_{TE}:

$$H_z \sim 1 + k_{0,\perp} W_{\mathrm{TE}}, \tag{28}$$

where

$$k_{0,\perp} \sim \omega\left[\varepsilon_0\varepsilon_{\mathrm{r}}\mu_0\mu_{\mathrm{r}} - \frac{1}{2}\left(\frac{\gamma}{\omega}\right)^2\right]$$

is the quasi-static wavenumber.

On the other hand, in the T.M. case it is shown in Poulton *et al.* (2001) that

$$E_z \sim 1 + k_{0,\perp} W_{\mathrm{TM}}, \tag{29}$$

where

$$\Delta W_{\mathrm{TM}} = 0, \quad \text{in } Y\backslash\bar{C}, \tag{30}$$

which is supplied with Bloch conditions on opposite sides of Y and some Neumann boundary condition $\partial W_{\mathrm{TM}}/\partial n = 0$ on the boundary ∂C.

Remarkedly, the electrostatic solutions $W_{\mathrm{TE},x}$ and $W_{\mathrm{TM},y}$ (repectively corresponding to fields directed along the x- and y-axes) form a Cauchy-Riemann pair and are related by Keller's theorem (Keller, 1964) according to $\mathrm{grad}\, W_{\mathrm{TE},x} = -\mathbf{e}_z \times \mathrm{grad}[R(\pi/2)W_{\mathrm{TM},y}]$, where $R(\varphi)$ denotes a rotation by an angle φ. From this, it can be deduced that, in the quasi-static limit, the transverse field modes $\mathbf{E}_t$ and $\mathbf{H}_t$ (which are respectively proportional to $\mathbf{e}_z \times \mathrm{grad} W_{\mathrm{TE}}$ and $\mathrm{grad} W_{\mathrm{TM}}$) form a linearly independent (orthogonal) pair of TEM modes, identical up to a rotation through angle $\pi/2$.

Actually, for a square array of circular metallic inclusions, it can be shown that the potential W_{TE} solution of equation (27) can be expressed as

$$W_{\mathrm{TE}} = A \ln(r/r_{\mathrm{c}}) + B, \tag{31}$$

where A and B are some integration constants deduced from the boundary conditions (quasi-periodicity of W on opposite sides of the basic cell Y as well as vanishing normal derivative on the boundary $r = r_c$).

2.2 Multipole expansions and boundary conditions

We expand the longitudinal fields E_z and H_z in terms of Bessel functions between the inclusions:

$$\xi_z = \sum_{m=-\infty}^{+\infty} \left[a_m^{\xi} J_m(k_\perp r) e^{im\Phi} + b_m^{\xi} Y_m(k_\perp r) \right] e^{im\Phi}, \quad \forall \xi \in \{E, H\}, \tag{32}$$

where r and Φ denote the radial and angular variables of E_z and H_z.

We derive from equations (20), (22) and (32) that the multipole coefficients a_m^{ξ} and b_m^{ξ} are linked by the boundary conditions

$$a_m^E = -\frac{Y_m(k_\perp r_c)}{J_m(k_\perp r_c)} b_m^E, \quad a_m^H = -\frac{Y'_m(k_\perp r_c)}{J'_m(k_\perp r_c)} b_m^H. \tag{33}$$

2.3 Quasi-periodic Green's function and Lattice sums

Another relation between the multipole coefficients can be gained by examining the structure of the lattice. This amounts to taking into account the quasi-periodicity of the transverse field (electric or magnetic), as stated by equation (23). Therefore, we introduce a two-dimensional quasi-periodic Green's function $G_{\mathbf{k}}$ which satisfies

$$(\Delta + k_\perp^2) G_{\mathbf{k}}(\mathbf{r}, \mathbf{r}') = \sum_{\mathbf{p} \in \mathbf{Z}^2} \delta(\mathbf{r} - \mathbf{r}' - \mathbf{R_p}) e^{i\mathbf{k}\cdot\mathbf{R_p}}, \tag{34}$$

where the sum stretches over the entire array of nodes $\mathbf{p}$ (locations of the centers of the cavities).

Using the Graf's addition theorem for Bessel functions, one can derive the representation of the Green's function $G_{\mathbf{k}}$ as a Neumann series within the central unit cell (Movchan *et al.*, 2002)

$$G_{\mathbf{k}}(\mathbf{r}, \mathbf{r}') = \frac{1}{4} Y_0(k_\perp |\mathbf{r} - \mathbf{r}'|) + \frac{1}{4} \sum_{l=-\infty}^{+\infty} S_l^Y(k_\perp, \mathbf{k}) J_l(k_\perp |\mathbf{r} - \mathbf{r}'|) e^{-il\theta}, \tag{35}$$

where the dynamic lattice sums S_l^Y are defined by

$$S_l^Y(k_\perp, \mathbf{k}) = \sum_{\mathbf{p} \in \mathbf{Z}^2 \setminus (0,0)} Y_l(k_\perp |\mathbf{R_p}|) e^{i\Phi_{\mathbf{p}} l + i\mathbf{k}\cdot\mathbf{R_p}}, \tag{36}$$

and $\Phi_{\mathbf{p}} = \arg(\mathbf{R_p})$, $\theta = \arg(\mathbf{r} - \mathbf{r}')$. As this series is slowly convergent, we shall use the following formula, derived by McPhedran and Dawes (1992) to calculate the lattice sums

$$S_l^Y(k_\perp,\mathbf{k})J_{l+q}(k_\perp z)=-\delta_{l0}\left[Y_q(k_\perp z)+\frac{1}{\pi}\sum_{n=1}^{q}\frac{(q-n)!}{(n-1)!}\left(\frac{2}{k_\perp z}\right)^{q-2n+2}\right]$$
$$-\frac{4i^l}{A}\sum_{\mathbf{p}\in\mathbf{Z}^2}\left(\frac{k_\perp}{|\mathbf{Q_p}|}\right)^q\frac{J_{l+q}(|\mathbf{Q_p}|z)\mathrm{e}^{\mathrm{i}l\theta_\mathbf{p}}}{|\mathbf{Q_p}|^2-(k_\perp)^2}, \tag{37}$$

where $A=|\mathbf{a}_1\times\mathbf{a}_2|$ denotes the area of the unit cell. For analytic purposes, it is convenient to use the values $\mathbf{p}=\mathbf{0}$, $z=\sqrt{A}=d$ (remember that d is the pitch of the direct array). The above formula is characterized by faster convergence via integration with respect to z. The integer parameter q gives the number of times the convergence of the lattice sums has been accelerated through integration and is thus called convergence acceleration index. The reciprocal unit cell is defined by the vectors[1]

$$\mathbf{a}^1=2\pi\frac{\mathbf{a}_2\times\mathbf{e}_z}{A},\quad \mathbf{a}^2=2\pi\frac{\mathbf{e}_z\times\mathbf{a}_1}{A}, \tag{38}$$

with the reciprocal lattice vectors

$$\mathbf{Q_p}=p_1\mathbf{a}^1+p_2\mathbf{a}^2+\mathbf{k},\quad \theta_\mathbf{p}=\arg(\mathbf{Q_p}). \tag{39}$$

The lattice sums satisfy the identity

$$S_{-l}^Y(k_\perp,\mathbf{k})=\overline{S_l^Y}(k_\perp,\mathbf{k}), \tag{40}$$

and hence it is sufficient to calculate them only for nonnegative values of l (here $\bar{\cdot}$ denotes the complex conjugate quantity).

2.4 Rayleigh identities and Rayleigh system

In equating the nonsingular field in the central unit cell with the superposed effect of all the other (singular) sources in the array, we obtain the following Rayleigh identities (Guenneau *et al.*, 2003) for every ξ in $\{E, K\}$,

$$a_l^\xi=\sum_{m=-\infty}^{+\infty}(-1)^{l+m}S_{m-l}^Y(k_\perp,\mathbf{k})b_m^\xi, \tag{41}$$

where the lattice sums $S_{m-l}^Y(k_\perp,\mathbf{k})$ provide the contribution of the lattice (Guenneau *et al.*, 2003). These two sets of equations are linked via boundary conditions equation (33) expressed in terms of multipoles and lead to the Rayleigh system (Guenneau *et al.*, 2003)

$$M_l^{\xi\xi}(k_\perp)b_l^\xi+\sum_{m=-\infty}^{+\infty}(-1)^{l+m}S_{m-l}^Y(k_\perp,\mathbf{k})b_m^\xi=0,\quad \forall\xi\in\{E,H\}, \tag{42}$$

where $M_l^{EE}=Y_l(k_\perp r_\mathrm{c})/J_l(k_\perp r_\mathrm{c})$ and $M_l^{HH}=Y_l'(k_\perp r_\mathrm{c})/J_l'(k_\perp r_\mathrm{c})$.

This algebraic system can be written as $\mathbf{RB}=(\mathbf{M}+\mathbf{S})\mathbf{B}$ where $\mathbf{R}(k_\perp,\mathbf{k})$ is the so-called Rayleigh matrix. It possesses standard properties of the Rayleigh system: it neatly separates the effect of the boundary conditions (the $M_l^{\xi\xi}$) from that of the geometry of the lattice (the S_l^Y), so that quite wide-ranging results can be gained without specifying particular compositions of voids. It is also remarked that the

coefficients $M_l^{\xi\xi}$ are real which makes **R** Hermitian due to equation (40). This is consistant with the fact that we consider lossless media.

2.5 Normalisation of the Rayleigh system

From the definition of the boundary terms $M_n^{\xi\xi}$, one can show that, as $n \to +\infty$,

$$M_n^{\xi\xi} = \mathcal{O}\left(\Gamma^2(n) n \left(\frac{1}{2} k_\perp r_c\right)^{-2n}\right) \tag{43}$$

Similarly, one can show that, for the lattice sums,

$$S_l^Y(k_\perp, \mathbf{k}) = \mathcal{O}\left(\Gamma(l)\left(\frac{1}{2} k_\perp d\right)^{-l}\right), \quad \text{as } l \to +\infty. \tag{44}$$

This causes numerical difficulties when

$$\frac{k_\perp d}{2} \ll 1,$$

since the off-diagonal terms increase extremely rapidly with index l:

$$z_l^\xi + \sum_{m=-\infty}^{+\infty} D_{lm}^{\xi\xi} z_m^\xi = 0, \quad \forall \xi \in \{E, H\}, \tag{45}$$

where

$$z_l^\xi = b_l^\xi \sqrt{|M_l^{\xi\xi}|}$$

and

$$D_{lm}^{\xi\xi} = \frac{\text{sign}\left(M_l^{\xi\xi}\right)}{\sqrt{\left|M_l^{\xi\xi}\right| |M_m|}} (-1)^{l+m} S_{m-l}^Y(k_\perp, \mathbf{k}) \text{ for } \xi \in \{E, H\}.$$

Using asymptotics of Bessel functions for large l and a fixed m, we get:

$$D_{lm}^{\xi\xi} = \mathcal{O}\left(\frac{(k_\perp r_c)^l}{\sqrt{\Gamma^2(l) l}} \frac{\Gamma(l-m)}{(k_\perp d)^l}\right) = \mathcal{O}\left(\frac{1}{\sqrt{l}} \left(\frac{r_c}{d}\right)^l \frac{(l-m)!}{l!}\right). \tag{46}$$

Therefore, if m is fixed as $l \to +\infty$,

$$D_{lm}^{\xi\xi} = \mathcal{O}\left(\frac{l^{-m}}{\sqrt{l}} \left(\frac{r_c}{d}\right)^l\right). \tag{47}$$

With l and m playing a symmetric role, it is a straightforward matter to show that, if l is fixed as $m \to +\infty$,

$$D_{lm}^{\xi\xi} = \mathcal{O}\left(\frac{m^{-l}}{\sqrt{m}} \left(\frac{r_c}{d}\right)^m\right). \tag{48}$$

Owing to this normalisation, the elements in the Rayleigh system decay exponentially away from the main diagonal, giving rise to higher multipole coefficients that decay similarly quickly. The frequency of vibration ω can be calculated for any given value of the Bloch vector $\mathbf{k}$ by annulling the determinant of the system $\det(\mathbf{R}(k_\perp, \mathbf{k}))$ at fixed conical parameter γ. In this way one can specify the dispersion relation for high frequencies by taking some high-order truncations (Guenneau *et al.*, 2003). Also, in the dilute composite limit, one can truncate the system to the dipole order ($l, m \in \{-1, 0, 1\}$) to get some effective properties in the long-wavelength limit.

3. Finite element method

3.1 Operator formulation

The following operators are defined:

$$\begin{cases} \mathrm{grad}_\gamma\, \varphi\,(x,y) = \mathrm{grad}\,(\varphi(x,y)\mathrm{e}^{\mathrm{i}\gamma z})\mathrm{e}^{-\mathrm{i}\gamma z} \\ \mathrm{curl}_\gamma\, \mathbf{V}\,(x,y) = \mathrm{curl}\,(\mathbf{V}(x,y)\mathrm{e}^{\mathrm{i}\gamma z})\mathrm{e}^{-\mathrm{i}\gamma z} \\ \mathrm{div}_\gamma\, \mathbf{V}(x,y) = \mathrm{div}\,(\mathbf{V}(x,y)\mathrm{e}^{\mathrm{i}\gamma z})\mathrm{e}^{-\mathrm{i}\gamma z} \end{cases} \tag{49}$$

Their domains are classes of ($\mathbf{k}$,Y)-periodic (i.e. satisfying equation (23)) square integrable functions with values in $\mathbb{C}$ (for grad_γ) or $\mathbb{C}^3$ (for div_γ and curl_γ) which we denote as $L^2_\sharp(\mathbf{k}, Y)$ and $[L^2_\sharp(\mathbf{k}, Y)]^3$.

We say that the couple ($\mathbf{E}_\mathbf{k}$,$\mathbf{H}_\mathbf{k}$) associated with the Bloch vector $\mathbf{k}$ is an electromagnetic Bloch wave if ($\mathbf{E}_\mathbf{k}$,$\mathbf{H}_\mathbf{k}$) verifies equation (1) and is of the form specified by equation (2) with

$$\begin{cases} (\gamma, \omega, \mathbf{k}) \in \mathbb{R}_+ \times \mathbb{R}_+ \times \mathbb{R}^2 \\ (\mathbf{E}_\mathbf{k}, \mathbf{H}_\mathbf{k}) \neq (\mathbf{0}, \mathbf{0}) \\ \mathbf{E}_\mathbf{k}, \mathbf{H}_\mathbf{k} \in [L^2_\sharp(\mathbf{k}, Y)]^3. \end{cases} \tag{50}$$

The solutions $(\mathbf{E}_\mathbf{k}, \mathbf{H}_\mathbf{k})$ of the spectral problem defined by equations (1), (2) and (23) hence satisfy

$$\begin{cases} \mathrm{curl}_\gamma \mathbf{H}_\mathbf{k} = -\mathrm{i}\omega\varepsilon_0\varepsilon_\mathrm{r}(x,y)\mathbf{E}_\mathbf{k} \\ \mathrm{curl}_\gamma \mathbf{E}_\mathbf{k} = \mathrm{i}\omega\mu_0\mu_\mathrm{r}(x,y)\mathbf{H}_\mathbf{k} \end{cases} \tag{51}$$

with ε_r and μ_r defined as in equation (1). Note that $\mathrm{curl}_\gamma \mathrm{grad}_\gamma \varphi = 0$ for smooth scalar fields φ and $\mathrm{div}_\gamma \mathrm{curl}_\gamma \mathbf{U} = 0$ for smooth vector fields $\mathbf{U}$.

Since we consider a (perfectly conducting) metallic inclusion C in the basic cell Y, the presence of metallic walls introduces unknown currents equal to the tangential component of the magnetic field. Therefore, we choose an electric field formulation to deal with simple boundary conditions (the tangential component of the electric field is null on metallic walls). Eliminating the magnetic field from equation (51), one finds:

$$\frac{1}{\varepsilon_r}\,\mathrm{curl}_\gamma\,\frac{1}{\mu_\mathrm{r}}\,\mathrm{curl}_\gamma \mathbf{E}_\mathbf{k} = k_0^2 \mathbf{E}_\mathbf{k} \tag{52}$$

where $k_0^2 = \varepsilon_o \mu_o \omega^2 = \omega^2/c^2$, c is the celerity of light in vacuum.

3.2 Weak formulation

The numerical formulation is given by the following residue (Guenneau *et al.*, 2002)

$$\begin{aligned}\mathscr{R}(\gamma;\mathbf{E}_{\mathbf{k}},\mathbf{E}'_{\mathbf{k}}) = \int_{Y\setminus\bar{C}} \mu_r^{-1}(&\mathrm{curl}_t\,\mathbf{E}_{t,\mathbf{k}}\cdot\mathrm{curl}_t\,\overline{\mathbf{E}}'_{t,\mathbf{k}} + \mathrm{grad}_t\,E_{l,\mathbf{k}}\cdot\mathrm{grad}_t\,\overline{E}'_{l,\mathbf{k}}\\ &- \mathrm{i}\,\gamma\,\mathbf{E}_{t,\mathbf{k}}\cdot\mathrm{grad}_t\,\overline{E}'_{l,\mathbf{k}} + i\gamma\,\mathrm{grad}_t\,E_{l,\mathbf{k}}\cdot\overline{\mathbf{E}}'_{t,\mathbf{k}} + \gamma^2\,\mathbf{E}_{t,\mathbf{k}}\cdot\overline{\mathbf{E}}'_{t,\mathbf{k}})\mathrm{d}x\,\mathrm{d}y \qquad (53)\\ &- k_0^2\int_{Y\setminus\bar{C}} \varepsilon_r(\mathbf{E}_{t,\mathbf{k}}\cdot\overline{\mathbf{E}}'_{t,\mathbf{k}} + E_{l,\mathbf{k}}\overline{E}'_{l,\mathbf{k}})\mathrm{d}x\,\mathrm{d}y.\end{aligned}$$

The weight vector field $\mathbf{E}'_{\mathbf{k}}$ is chosen in the same discrete Hilbert space as the unknown field $\mathbf{E}_{\mathbf{k}}$, i.e. a space with finite dimension equal to the number of numerical parameters to be determined. This formulation involves both a transverse field $\mathbf{E}_{t,\mathbf{k}}$ in the section of the guide and a longitudinal field $E_{l,\mathbf{k}}$ along its axis such that:

$$\mathbf{E}_{\mathbf{k}} = \mathbf{E}_{t,\mathbf{k}} + E_{l,\mathbf{k}}\mathbf{e}_z. \qquad (54)$$

3.3 Discrete weak form

The section of the guide is meshed with triangles and Whitney finite elements (Bossavit, 1990) are used, i.e. edge elements for the transverse field and node elements for the longitudinal field:

$$\mathbf{E}_{\mathbf{k}} = \begin{cases}\mathbf{E}_{t,\mathbf{k}} = \sum\limits_{\text{edges}\,i} \alpha_i\mathbf{w}_i^{\mathbf{e}}(x,y)\\ E_{l,\mathbf{k}} = \sum\limits_{\text{nodes}\,j} \gamma_j w_j^n(x,y)\end{cases} \qquad (55)$$

where α_i denotes the line integral of the transverse component $\mathbf{E}_{t,\mathbf{k}}$ on the edges, and γ_j denotes the line integral of the longitudinal component $E_{l,\mathbf{k}}$ along one unit of length of the axis of the guide (what is equivalent to a nodal value). Besides, $w_j^n(x,y) = \lambda_j(x,y)$ and $\mathbf{w}_i^{\mathbf{e}}(x,y) = \lambda_k(x,y)\mathrm{grad}\,\lambda_l(x,y) - \lambda_l(x,y)\mathrm{grad}\,\lambda_k(x,y)$ (where λ_j is the barycentric coordinate of node j and the edge i has nodes k and l as extremities) are, respectively, the basis functions of Whitney 1-forms (edge element discrete space W^1) and Whitney 0-forms (nodal element discrete space W^0).

Moreover, the use of the Whitney elements solves the spurious mode problem in a way similar to the one of the cavities (Bossavit, 1990).

As the eigenvalue problem involves, on the one side, k_0^2 only and, on the other side, both γ and γ^2, a more classical (though generalized) eigenvalue problem is obtained by fixing $\gamma \in \mathbb{R}_+$ (rather than k_0^2) for a given Bloch vector $\mathbf{k}$ and looking for $(k_0^2, \mathbf{E}_{\mathbf{k}})$ satisfying the discrete spectral problem.

3.4 Implementation of Bloch conditions

In order to find Bloch modes with the finite element method, some changes have to be performed with respect to classical boundary value problems that will be named Bloch conditions (Nicolet *et al.*, 2004). To avoid tedious notations, a simpler case is considered here: a scalar field $U_{\mathbf{k}}(x, y)$ (time and z dependence are irrelevant here and there is no particular problem to extend this method to vector quantities and edge elements) on the square cell Y with Bloch conditions relating the left and the right side. The set of nodes is separated in three subsets: the nodes on the left side, i.e. with $x = 0$, corresponding to

the column array of unknowns $\mathbf{u_l}$, the nodes on the right side, i.e. with $x = 1$, corresponding to the column array of unknowns $\mathbf{u_r}$, and the internal nodes, i.e. with $x \in [0, 1]$, corresponding to the column array of unknowns $\mathbf{u}$. One has the following structure for the matrix problem (corresponding in fact to natural boundary conditions, i.e. Neumann homogeneous boundary conditions):

$$\mathbf{A}\begin{pmatrix}\mathbf{u}\\ \mathbf{u_l}\\ \mathbf{u_r}\end{pmatrix} = \mathbf{b} \tag{56}$$

where $\mathbf{A}$ is the (square Hermitian) matrix of the system and $\mathbf{b}$ the second member column array. The solution to be approximated by the numerical method is a Bloch function $U_{\mathbf{k}}(x,y) = U(x,y)\mathrm{e}^{\mathrm{i}(k_x x + k_y y)}$ with U Y-periodic and in particular $U(x+1,y) = U(x,y)$. Therefore, the relation between the left and the right side is:

$$U_{\mathbf{k}}(1,y) = U(1,y)\mathrm{e}^{\mathrm{i}(k_x + k_y y)} = U_{\mathbf{k}}(0,y)\mathrm{e}^{\mathrm{i}k_x} \Rightarrow \mathbf{u_r} = \mathbf{u_l}\mathrm{e}^{\mathrm{i}k_x} \tag{57}$$

Therefore, the set of unknowns can be expressed in function of the reduced set $\mathbf{u}$ and $\mathbf{u_l}$ due to:

$$\begin{pmatrix}\mathbf{u}\\ \mathbf{u_l}\\ \mathbf{u_r}\end{pmatrix} = \mathbf{P}\begin{pmatrix}\mathbf{u}\\ \mathbf{u_l}\end{pmatrix} \quad \text{with } \mathbf{P} = \begin{pmatrix}\mathbf{1} & \mathbf{0}\\ \mathbf{0} & \mathbf{1}\\ \mathbf{0} & \mathbf{1}\mathrm{e}^{\mathrm{i}k_x}\end{pmatrix} \tag{58}$$

where $\mathbf{1}$ and $\mathbf{0}$ are identity and null matrices, respectively, with suitable dimensions. The finite element equations related to the eliminated nodes have now to be taken into account. Owing to periodicity of the structure, the element on the left of the right side corresponds to elements on the left of the left side. Therefore their contributions (i.e. equations corresponding to $\mathbf{u_r}$) must be added to the equations corresponding to $\boldsymbol{u_l}$ with the correct phase factor, i.e. $\mathrm{e}^{-\mathrm{i}k_x}$ what amounts to multiplying the system matrix by $\mathbf{P}^*$, i.e. the Hermitian conjugate of $\mathbf{P}$. Finally, the linear system to be solved is:

$$\mathbf{P}^*\mathbf{A}\mathbf{P}\begin{pmatrix}\mathbf{u}\\ \mathbf{u_l}\end{pmatrix} = \mathbf{P}^*\mathbf{b} \tag{59}$$

where it is worth noting that the system matrix is still Hermitian what is important for numerical computation. Now a generalized eigenvalue problem (with natural boundary conditions) $\mathbf{A}\mathbf{u} = \lambda\mathbf{B}\mathbf{u}$ is transformed to a Bloch mode problem according to $\mathbf{P}^*\mathbf{A}\mathbf{P}\mathbf{u}' = \lambda\mathbf{P}^*\mathbf{B}\mathbf{P}\mathbf{u}'$. Such problems involving large sparse Hermitian matrices can be solved using Lanczos algorithm that gives the largest eigenvalues (Nicolet *et al.*, 2004). Physically we are in fact interested in the smallest eigenvalues and therefore $\mathbf{A}^{-1}$, the inverse of $\mathbf{A}$, instead of $\mathbf{A}$ itself must be used in the iterations. Of course, the inverse is never computed explicitly but the matrix-vector products are replaced by system solutions due to a GMRES method. It is therefore obvious that the numerical efficiency of the process relies strongly on Krylov subspace techniques and the Arnoldi iteration algorithm (Nicolet *et al.*, 2004). The practical implementation of the model has been performed thanks to the GetDP software (Dular *et al.*, 1998) (Figure 2).

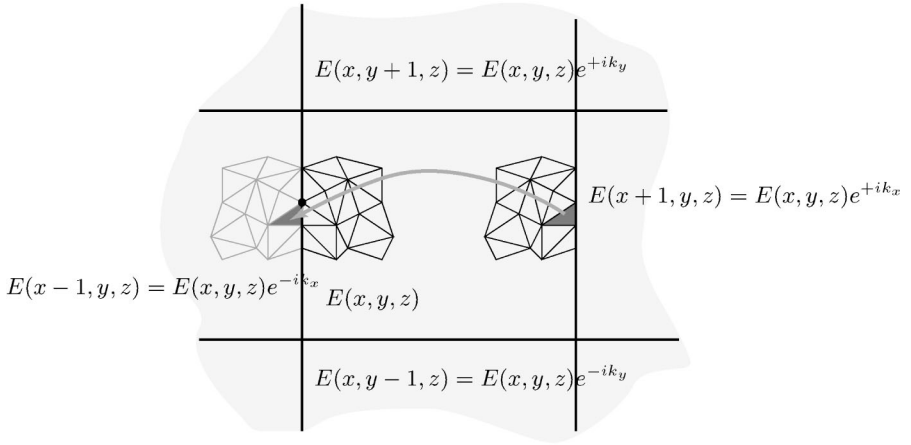

Figure 2.
The Bloch theorem and virtual periodic meshing

4. Numerical results

In this section, we provide some numerical illustration for an array of channels filled with perfect metal (any metal in the microwave regime) which are drilled within a silica matrix in a densely packed configuration. We obtain some band diagrams exhibiting a nice photonic bandgap, i.e. a range of frequencies where no electromagnetic wave propagates (Figures 3 and 4). When we remove one channel, we observe some localised signal sitting right in the middle of the gap (its normalised frequency $\omega d/c = 7.95$ is independent of the Bloch vector $\mathbf{k}$). The practical application lies in futurist optical fibres (Knight *et al.*, 1999; Zolla *et al.*, 2004).

4.1 Effective properties and singular perturbation

On the dispersion diagrams of Figures 3 and 4, we can only see one acoustic band. The reason for this is that if we consider $k_\perp r_c \ll 1$ in equation (42), the relationship between $k_\perp$ and $\mathbf{k}$ is supplied by

$$M_0^{\xi\xi}(k_\perp r_c) + S_l^Y(k_\perp, \mathbf{k}) = 0, \quad \forall \xi \in \{E, H\}. \tag{60}$$

This equation provides the first perturbation away from the plane-wave state. It appears to hold true even for shorter wavelengths in comparison with the array spacing d, as long as $k_\perp r_c \ll 1$. Now, for long-wavelengths, it is possible to obtain analytic expressions for the lattice sums S_l^Y in equation (37). We find that when $k_\perp \to |\mathbf{Q_m}|$, equation (60) can be approximated as (Guenneau *et al.*, 2003)

$$\begin{aligned} M_0^{\xi\xi}(|\mathbf{Q_m}| r_c) - \frac{2}{\pi}\left[\ln\left(\frac{|\mathbf{k}|}{2}\right) + \chi_1\right] - 4\left(\chi_2 + \frac{\ln(2d)}{\pi}\right) \\ - \frac{4}{d^2}\frac{1}{|\mathbf{Q_m}|^2 - k_\perp^2} \sum_{|\mathbf{Q_n}|=|\mathbf{Q_m}|} 1 + O(||\mathbf{Q_m}| - k_\perp|) = 0, \end{aligned} \tag{61}$$

where $\chi_1 \simeq -0.318895593$, χ_2 is the Euler's constant 0.557215665 and $\mathbf{Q_m}$ is defined by equation (39). Hence, the boundary term M_0^{HH} in equation (61) becomes

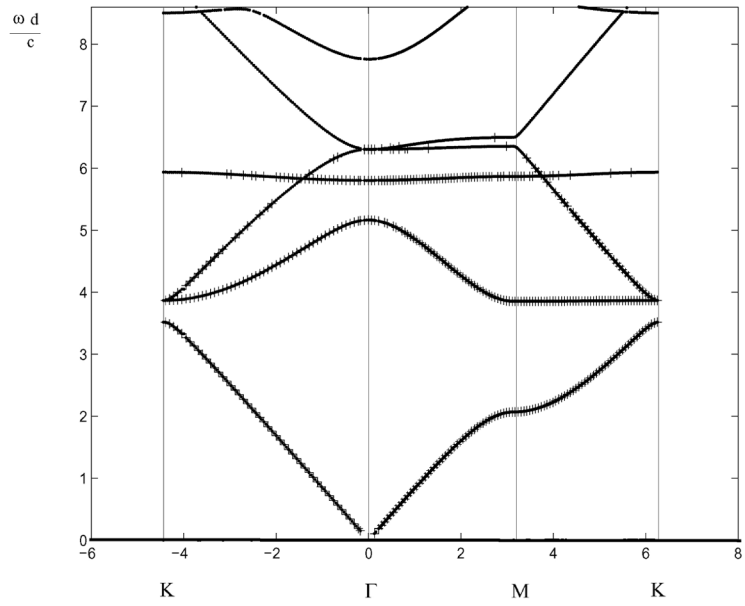

Notes: The propagation constant is $\gamma = 0\mu m^{-1}$ (transverse case). On the vertical axis we represent the normalised frequency *wd/c* and on the positive part of the horizontal axis the modulus *k* of the Bloch vector in μm^{-1} (respectively $-k$ on the negative part of the horizontal axis). Γ, *M*, *K* represent the nodes (0, 0), (0, π/d), (π/d, π/d) of the irreducible part of the Brillouin zone described by **k**. The crosses '+' correspond to finite element modeling whereas the dots '.' are given by the Rayleigh method

Figure 3.
The propagation constant is $\gamma = 0\mu m^{-1}$ (transverse case). Band diagram for a periodic array of cavities arranged on a square lattice (radius 0.35 μm, center spacing $d=1$ μm) in a matrix of silica ($\varepsilon_r = 1.5$)

$$M_0^{HH} = \frac{Y_0'(|\mathbf{Q_m}|r_c)}{J_0'(|\mathbf{Q_m}|r_c)} = -\frac{1}{\pi}\left(\frac{2}{|\mathbf{Q_m}|r_c}\right)^2 + O((|\mathbf{Q_m}|r_c)^0), \tag{62}$$

and so this term (corresponding to TE polarised waves) dominates the perturbation in equation (61). It corresponds in fact to the first dispersion curve.

On the dispersion diagram, we can only see one acoustic band. The reason for this is that if we consider $k_\perp r_c \ll 1$ in equation (61), the boundary term M_0^{EE} becomes

$$M_0^{EE} = \frac{Y_0(|\mathbf{Q_m}|r_c)}{J_0(|\mathbf{Q_m}|r_c)} = -\frac{2}{\pi}(\ln(|\mathbf{Q_m}|r_c) + \chi_2) + O((|\mathbf{Q_m}|r_c)^2), \tag{63}$$

and so this term (corresponding to TM polarised waves) is of the same order as the contribution of lattice sums in equation (61). In this case, equation (61) becomes

$$k^2 - k_\perp^2 = \frac{2\pi}{d^2}\left(\ln\frac{r_c}{d} + C\right)^{-1}, \tag{64}$$

where $C = -2\pi\chi_1 - 2\ln 2 \simeq 1.31053292$. This corresponds in fact to the fourth dispersion curve. Also, we note that the acoustic curve $\omega(\mathbf{k})$ is quadratic in the neighbourhood of the origin in Figure 4 which is not the case in Figure 3. This can be also classified as a singular perturbation induced by the conical parameter γ. For small γ, the asymptotics of eigenfrequencies take the following form:

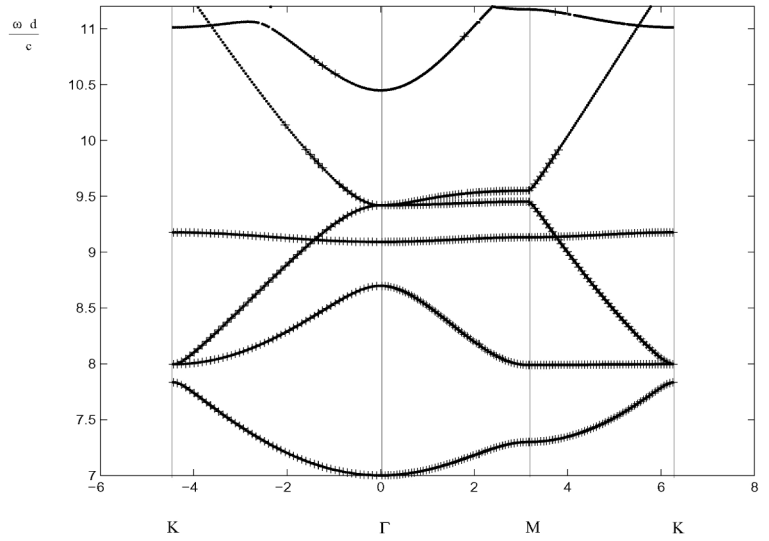

Figure 4.
The propagation constant is $\gamma = 7\mu\text{m}^{-1}$ (conical case). Band diagram for a periodic array of cavities arranged on a square lattice (radius 0.35 μm, center spacing d=1 μm) in a matrix of silica ($\varepsilon_r = 1.5$)

Notes: The propagation constant is $\gamma = 7\mu\text{m}^{-1}$ (conical case). On the vertical axis we represent the normalised frequency *wd/c* and on the positive part of the horizontal axis the modulus *k* of the Bloch vector in μm^{-1} (respectively *–k* on the negative part of the horizontal axis). Γ, *M*, *K* represent the nodes (0, 0), (0, π/*d*), (π/*d*, π/*d*) of the irreducible part of the Brillouin zone described by **k**. The crosses '+' correspond to finite element modeling whereas the dots '.' are given by the Rayleigh method

$$\omega(\mathbf{k}, \gamma) \sim \omega_0(\mathbf{k}) + \gamma\omega_1(\mathbf{k}/\gamma), \tag{65}$$

so that the increment of the frequency may be small, whereas the (transverse) group velocity $\partial\omega/\partial k$ may change by a finite increment. This characterises the presence of noncommuting limit, namely between $\omega \to 0$ and $\gamma \to 0$, which is discussed in (Poulton *et al.*, 2004).

In transverse incidence ($\gamma = 0$) and for reasons of symmetry, it appears that in the neighbourhood of the origin $\mathbf{k} = (0, 0)$, the frequency ω is written as per:

$$\omega = v|\mathbf{k}| + \mathcal{O}(k_x, k_y), \tag{66}$$

and the effective index is given by $N^{\text{eff}} = c/v$ (see straight line going to the origin in Figure 3). But in oblique incidence ($\gamma > 0$), it is clear from Figure 4 that the effective refractive index N^{eff} is no longer given by the variation of group velocity at the origin. It is in fact connected to the notion of effective mass (second order derivatives) (Guenneau *et al.*, 2003).

4.2 Photonic band gaps for square periodic arrays

The complete gap occurs only for TE waves (since there is no acoustic band for TM waves). The second dispersion curve corresponds indeed to TE waves and it is called optical band. We observe that the group velocity can be negative in the neighbouhrood of Γ. This can be associated to a negative effective refractive index which possibly leads to newly discovered left-handed-materials (Smith *et al.*, 2004).

4.3 Localised modes associated with periodic multiple defects

As a simple illustration, we start with the removal of the central channel within a supercell containing 7×7 voids of the micro-structured fibre. We set some Bloch conditions on opposite sides of this supercell, thereby assuming some infinite extent of the PCF in the transverse plane ($x-y$). We then observe in Figure 5 a new eigenstate

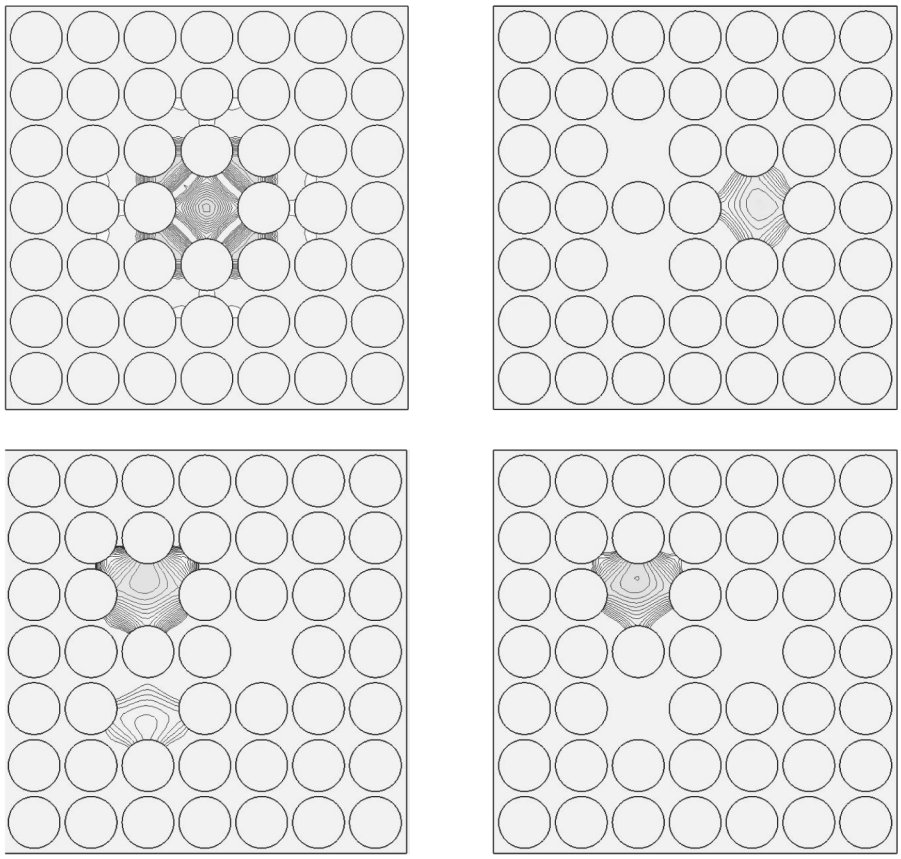

Notes: Upper-Left: Localised mode for the PCF corresponding to Figure 4, when we remove one cavity (real part of the longitudinal electric field for a null Bloch vector $E_{\mathrm{l},\,\mathbf{0}}$). The normalised frequency of this signal is $\omega d/c = 7.95$. Upper-right and lower-left (clockwise): real part of the longitudinal electric field $E_{l,\pi}$ (TM wave) for a Bloch vector $\mathbf{k} = (\pi, \pi)$ associated with the normalised eigenfrequencies $\omega d/c = 7.91$ (twofold degenerated modes) and $\omega d/c = 7.99$ for a given normalised propagation constant $\gamma d = 7.0$ and a square periodic array of pitch $d = 1\mu$m consisting of circular cylindrical metallic cylinders of radius $r_c/d = 0.35 = 0.35$. Here, we have removed three cylinders (hence sculpting three 'high-index defects'). These frequencies remain unchanged when the normalised Bloch vector $\mathbf{k}d$ describes ΓMK, A linear combination of the aforementioned modes governs the phenomenon of 'cross-talk' between the upper-left, lower-left and right cores (Guenneau *et al*., 2001 for detailed analysis of cross-talk between optical waveguides)

Figure 5.
Models for periodic structures with defects

associated with an eigenfrequency sitting within the band gap of Figure 4. We note that this corresponds to a flat narrow pass-band on a corresponding dispersion diagram (not depicted since the number of dispersion curves increases dramatically with the size of the supercell) as checked numerically, this pass-band does not depend on the orientation of the Bloch vector within the first Brillouin zone ΓMK. The reader may argue that the Bloch conditions assumed on the opposite sides of the basic cell will influence the result. Even though our modelling does not contain within it all the physics at work (for instance, we cannot compute the leakage of the localised mode), we observe that removing any of the channels within the macrocell does not affect the eigenfrequency and associated eigenstate: this is a numerical evidence of the well-behaved convergence of the finite element algorithm for Bloch conditions.

We now move to the richer case of multiple defects within the macrocell. Provided that the cores are close enough, they start to talk to each other (Figure 5). This phenomenon is fairly well known in the field of optical waveguides (Guenneau *et al.*, 2001), but its extension to microstructured fibres is new and presents exciting applications in multiplexing/demultiplexing as was foreseen in the transverse case by Centeno *et al.* (1999).

5. Conclusion

In this paper, we have presented two algorithms by which one can construct some band diagrams associated with conical Bloch waves in arrays of metallic cylinders. The first one, the so-called Rayleigh method, is an analytic algorithm well suited for various asymptotic purposes such as the long-wavelength limit (homogenisation) and leads to an infinite algebraic system which is typically truncated as a 22×22 matrix. The second one, the so-called finite element method, leads to large sparse systems, but can tackle problems of more complex geometries (such as arrays of cylinders of arbitrary cross-section or models for periodic structures with defects as in Figure 5).

Note

1. We note that the dot product $\mathbf{k} \cdot \mathbf{R_p}$ in equations (23), (34) and (36) is nothing else but a duality product, hence we adopt covariant/contravariant notations for the lattice vectors in physical and reciprocal spaces.

References

Bossavit, A. (1990), "Solving Maxwell equations in a closed cavity, and the question of spurious modes", *IEEE Trans. Magn.*, Vol. 26 No. 2, p. 702.

Centeno, E., Guizal, B. and Felbacq, D. (1999), "Multiplexing and demultiplexing with photonic crystals", *J. Opt. A, Pure Appl. Opt.*, Vol. 1 No. 5, p. L10.

Dular, P., Geuzaine, C., Henrotte, F. and Legros, W. (1998), "A general environment for the treatment of discrete problems and its application to the finite element method", *IEEE Trans. Mag.*, Vol. 34 No. 5, pp. 3395, available at: www.geuz.org

Guenneau, S., Nicolet, A., Zolla, F., Geuzaine, C. and Meys, B. (2001), "A finite element formulation for spectral problems in optical fibers", *COMPEL, The International Journal For Computation and Mathematics in Electrical and Electronic Engineering*, Vol. 20 No. 1, p. 120.

Guenneau, S., Nicolet, A., Zolla, F. and Lasquellec, S. (2002), "Modeling of photonic crystal optical fibers with finite elements", *IEEE Trans. Mag.*, Vol. 38 No. 2, p. 1261.

Guenneau, S., Poulton, C.G. and Movchan, A.B. (2003), "Oblique propagation of electromagnetic and elastic waves for an array of cylindrical fibres", *Proc. Roy. Soc. Lond. A*, Vol. 459, p. 2215.

Keller, J.B. (1964), "On the conductivity of a composite medium", *J. Math. Phys.*, Vol. 5, p. 548.

Knight, J.C., Broeng, J., Birks, T.A. and Russell, P. St J. (1999), "Photonic band gap guidance in optical fibers", *Science*, Vol. 282, p. 1476.

McPhedran, R.C. and Dawes, D.H. (1992), "Lattices sums for a dynamic scattering problem", *J. Elect. Waves Appl.*, Vol. 6, p. 1327.

McPhedran, R.C., Nicorovici, N.A. and Botten, L.C. (1997), "The TEM mode and homogenization of doubly periodic structures", *J. Elect. Waves Appl.*, Vol. 11, p. 981.

Movchan, A.B., Movchan, N.V. and Poulton, C.G. (2002), *Asymptotic Models of Fields in Dilute and Densely Packed Composites*, Imperial College Press, London.

Nicolet, A., Guenneau, S., Geuzaine, C. and Zolla, F. (2004), "Modeling of electromagnetic waves in periodic media with finite elements", *Journal of Computational and Applied Mathematics*, Vol. 168 Nos 1/2, pp. 321-9.

Poulton, C.G., Guenneau, S. and Movchan, A.B. (2004), "Noncommuting limits and effective properties for oblique propagation of electromagnetic waves through an array of aligned fibres", *Phys. Rev. B*, Vol. 69 Nos 19, pp. 195112.

Poulton, C.G., Botten, L.C., McPhedran, R.C., Nicorovici, N.A. and Movchan, A.B. (2001), "Noncommuting limits in electromagnetic scattering: Asymptotic analysis for an array of highly conducting inclusions", *SIAM J. Appl. Math.*, Vol. 61, p. 1706.

Smith, D.R., Pendry, J.B., and Wiltshire, C.K. (2004), *Metamaterials and Negative Refractive Index Science*, Vol. 305, p. 788.

Zolla, F., Renversez, G., Nicolet, A., Kuhlmey, B., Guenneau, S. and Felbacq, D. (2004), *Foundations of Photonic Crystal Fibres*, Imperial College Press, London.

Further reading

Guenneau, S., Lasquellec, S., Nicolet, A. and Zolla, F. (2002), "Design of photonic band gap optical fibers using finite elements", *COMPEL, The International Journal For Computation and Mathematics in Electrical and Electronic Engineering*, Vol. 21 No. 4, p. 534.

White, T.P., Botten, L.C., McPhedran, R.C. and de Sterke, C.M. (2003), "Ultracompact resonant filters in photonic crystals", *Optics Letters*, Vol. 28, p. 2452.